*energies*

MDPI

*Article*

# Alternative Current Injection Newton and Fast Decoupled Power Flow

**Cristina Coutinho de Oliveira [1], Alfredo Bonini Neto [2], Dilson Amancio Alves [3], Carlos Roberto Minussi [3,*] and Carlos Alberto Castro [4]**

[1] Federal Institute of Amapá (IFAP), Pedra Branca do Amapari Center, Macapá 68945-000, Brazil
[2] School of Sciences and Engineering, São Paulo State University (Unesp), Tupã 17602-496, Brazil
[3] School of Engineering, São Paulo State University (Unesp), Ilha Solteira 15385-000, Brazil
[4] Technology Center, Pontifical Catholic University of Campinas (PUC), Campinas 13087-571, Brazil
* Correspondence: carlos.minussi@unesp.br

**Abstract:** This article presents an alternative Newton-Raphson power flow method version. This method has been developed based on current injection equations formulated in polar coordinates. Likewise, the fast decoupled power flow, elaborated using current injection (BX version), is presented. These methods are tested considering electrical power systems composed of 57-, 118-, and 300-bus, as well as a realistic system of 787-bus. For the robustness analysis, simulations were performed considering different loading conditions and R/X ratios of the transmission line. Based on the simulations that were realized, there is evidence that the performance of the proposed current injection methods is similar to the power injection methods.

**Keywords:** power flow analysis; current injection power flow; PV representation; polar coordinates

check for updates

**Citation:** Coutinho de Oliveira, C.; Bonini Neto, A.; Alves, D.A.; Minussi, C.R.; Castro, C.A. Alternative Current Injection Newton and Fast Decoupled Power Flow. *Energies* **2023**, *16*, 2548. https://doi.org/10.3390/en16062548

Academic Editor: Maria Grazia De Giorgi

Received: 23 January 2023
Revised: 24 February 2023
Accepted: 1 March 2023
Published: 8 March 2023

**Copyright:** © 2023 by the authors. Licensee MDPI, Basel, Switzerland. This article is an open access article distributed under the terms and conditions of the Creative Commons Attribution (CC BY) license (https://creativecommons.org/licenses/by/4.0/).

## 1. Introduction

The large number of papers related to power flow development that have been published over the last decades demonstrates its importance for the planning and operation analysis of electric power systems [1–9]. Fast convergence is one of the desired characteristics for application in contingency analysis and load margin determination, which requires high computational processing time, given the large number of cases to be processed and analyzed in these studies, particularly for real-time operation [10–12].

A survey on numerical techniques for power flow calculation is presented in [13]. Several formulations have been employed for the general equations of the power flow problem. Formulations of power flow equations can be expressed in polar or rectangular coordinates, or a combination of both [14]. It is a well-known fact that the Newton-Raphson method is the most used in the resolutions. A comprehensive review of power flow methods as tools for contingency analysis and steady-state voltage stability of a power system can be found in [9–12]. They may be based on the power or current injection balance and, in some cases, on a combination of both, which are called hybrids [4–9,13–16]. A number of formulations incorporating FACTS devices based on the current injection approach have been proposed in the literature, as it is considered more adequate for that purpose [6,7,17].

In the power or current injection balance formulation expressed in rectangular coordinates, an additional voltage-magnitude squared mismatch equation is needed for each PV bus, since its generated reactive power ($Q_{gen}$) is unknown [14]. Thus, despite the effort in reducing the computational burden associated with computing the Jacobian terms in the case of voltages represented in rectangular coordinates, the polar coordinates formulation is preferred, providing a smaller number of equations, once the reactive power mismatch equations related to PV buses are not considered (provided that their generated reactive power lies within their maximum and minimum limits) [13]. Besides, in the current injection balance formulation, the value of $Q_{gen}$ affects the real and imaginary current mismatches,

once it appears explicitly in both equations. Therefore, the appropriate representation of PV buses has been the main concern in the most current injection formulations. In [4], a current injection balance formulation expressed in polar coordinates using the Newton-Raphson method is presented. Its performance is compared to that of a standard power injection in polar coordinates. During the iterative process, to meet the limits of the PV-bus, the generated reactive power is kept unchanged, being updated before the next iteration. The use of current injection mismatches with reactive mismatch ΔQ as a dependent variable, together with a voltage magnitude constraint equation, both written in rectangular coordinates is proposed in [18–20]. A hybrid power flow method with PV buses represented by active power mismatch equations, using angle deviation as a variable, and PQ buses represented by equations of current injection written in rectangular coordinates is presented in [5,13,21]. In the modified current injection power flow formulation proposed in [8], the generated reactive power is a function of the state variables, the nodal voltage magnitudes, and phase angles. The results have shown an improvement of the iterative process convergence as a consequence of a more accurate calculation of the Jacobian elements, since they take into account the influence of generated reactive power variation when obtaining the correction vectors ($\Delta\theta$ and $\Delta|\mathbf{V}|$). In reference [22], an integrated analysis is proposed, which allows a single power flow method to be effectively applied to any voltage level of electric power systems. This methodology combines the decoupled power flow approach and the complex normalization technique to efficiently deal with the high dimension of the unified network analysis, as well as the different characteristics of the transmission and distribution networks, about the line parameters and topological arrangements. The obtained results show the effectiveness of the proposed approach and attest to the relevance of integrated power flow analyses to properly determine the interrelationships between the different levels of operation of the electrical network.

The objective of this paper is to present an alternative Newton-Raphson current injection model obtained from the current injection power flow equations in polar coordinates. Besides, a BX version of the current injection fast decoupled power flow, developed from the Newton-Raphson formulation, is also presented. Their performances are compared to those of their respective power injection versions through numerical simulations conducted for the 57-, 118-, and 300-bus IEEE test systems and for a realistic 787-bus system, corresponding to part of the South-Southeast Brazilian system. Different R/X transmission line ratios and loading conditions are taken into account for performance assessment purposes. The results obtained with the proposed Newton-Raphson current injection model exhibit good convergence characteristics, while the BX version performs similarly to its corresponding power injection version.

## 2. Alternative Newton-Raphson Current Injection Model

The current injections in the Newton-Raphson power flow formulation are expressed in complex polar coordinates [14]. The components, real ($\Delta G_k(\theta, |\mathbf{V}|)$) and imaginary ($\Delta HI_k(\theta, |\mathbf{V}|)$), of the complex current mismatch at a given bus k are given by [4,8,13]:

$$\begin{aligned} \Delta G_k(\theta, |\mathbf{V}|) &= \frac{|S_k^{sp}|}{|V_k|}\cos(-\varphi_k + \theta_k) - \sum_{i\in\kappa} |Y_{ki}||V_i|\cos(\phi_{ki} + \theta_i) = 0 \\ \Delta HI_k(\theta, |\mathbf{V}|) &= \frac{|S_k^{sp}|}{|V_k|}\sin(-\varphi_k + \theta_k) - \sum_{i\in\kappa} |Y_{ki}||V_i|\sin(\phi_{ki} + \theta_i) = 0 \end{aligned} \quad (1)$$

where κ is the set of buses directly connected to bus $k$ plus bus $k$ itself, $|V_k|$, $|V_i|$, $\theta_k$, and $\theta_i$ are the voltage magnitudes and angles at buses $k$ and $i$, $|Y_{ki}|$ and $\phi_{ki}$ are the magnitude and angle of element ($k$,$i$) of the nodal admittance matrix $\mathbf{Y}$, $\theta$ and $|\mathbf{V}|$ are the vectors of the nodal voltage phase angles and magnitudes, and $\theta_{ki} = \theta_k - \theta_i$ is the voltage phase angle difference between buses $k$ and $i$. In Equation (1), $\left|S_k^{sp}\right|$ and $\varphi_k$ are the respective magnitude and angle of the net specified complex power injected at bus $k$, given by:

$$S_k^{sp} = \left|S_k^{sp}\right|\cos(\varphi_k) + j\left|S_k^{sp}\right|\sin(\varphi_k) = \left(P_{gen,k}^{sp} - P_{load,k}^{sp}\right) + j\left(Q_{gen,k} - Q_{load,k}^{sp}\right) = P_k^{sp} + jQ_k^{sp} \quad (2)$$

where $P^{sp}_{gen,k}$ and $P^{sp}_{load,k}$ are, respectively, the specified active power generated and consumed for the load (PQ) and generation (PV) buses, and $Q^{sp}_{load,k}$ is the consumed reactive power specified for the PQ buses.

Equation (1) is appropriate for systems with PQ buses but not for systems with the presence of any PV bus whose generated reactive power is within its bounds, as in this case the generated reactive power ($Q_{gen,k}$) is not known a priori, i.e., it is an unknown variable. On the other hand, this variable can be eliminated from Equation (1) by rewriting it as follows:

$$\Delta G_k(\theta, |\mathbf{V}|) = \frac{P^{sp}_k}{|V_k|}\cos(\theta_k) + \frac{Q^{sp}_k}{|V_k|}\sin(\theta_k) - |Y_{kk}||V_k|\cos(\phi_{kk}+\theta_k) - \sum_{i\in\Omega_k}|Y_{ki}||V_i|\cos(\phi_{ki}+\theta_i) = 0 \quad (3)$$

$$\Delta H_k(\theta, |\mathbf{V}|) = \frac{P^{sp}_k}{|V_k|}\sin(\theta_k) - \frac{Q^{sp}_k}{|V_k|}\cos(\theta_k) - |Y_{kk}||V_k|\sin(\phi_{kk}+\theta_k) - \sum_{i\in\Omega_k}|Y_{ki}||V_i|\sin(\phi_{ki}+\theta_i) = 0 \quad (4)$$

where $\Omega_k$ is the set of buses directly connected to bus $k$. Adding Equation (3) multiplied by $\cos(\theta_k)$ to Equation (4) multiplied by $\sin(\theta_k)$ gives (refer to Appendix A):

$$\frac{\Delta P_k}{|V_k|} = \frac{P^{sp}_k}{|V_k|} - \sum_{i\in\kappa}|Y_{ki}||V_i|(\cos(\phi_{ki}-\theta_{ki})) = 0 \quad (5)$$

Note that Equation (5) multiplied by $|V_k|$ leads to the active power mismatch equation ($\Delta P_k = P^{sp}_k - |V_k|\sum_{i\in\kappa}|Y_{ki}||V_i|\cos(\phi_{ki}-\theta_{ki}) = 0$) of the standard power flow (SPF) formulation based on power injection [23]. Therefore, in the alternative Newton-Raphson formulation proposed in this paper, named as proposed current injection power flow (PCIPF), Equation (5) will be used for PV buses, while Equations (3) and (4) for PQ buses. It is worth noticing that the active power mismatches are naturally normalized during the derivation of Equation (5). In [24], a hybrid power flow formulation based on current and power balance equations written in rectangular coordinates was presented. This method is considered as a hybrid formulation, using the current balance Equation (6) for PQ buses, and the active power mismatch Equation (7) and voltage magnitude constraint, Equation (8), for PV buses was proposed. Note that this formulation can be obtained from algebraic manipulations of Equation (6). Adding the equation of ($\Delta G_k$(E,F)) multiplied by $E_k$ with that of ($\Delta H_k$(E,F)) multiplied by $F_k$ leads to the formulation proposed in [24]. In [5] a method using a combination of power and current injection power flow methods was proposed. It uses the current injection balance Equation (6) for PQ buses while for PV buses, the active power balance equation is used for the calculation of voltage angle ($\theta_k$), omitting in this case the voltage Equation (8).

$$\Delta G_k(\mathbf{E},\mathbf{F}) = \frac{\left(P^{sp}_k E_k + Q^{sp}_k F_k\right)}{\left(E_k^2+F_k^2\right)} - \sum_{m\in\kappa}(G_{km}E_m - B_{km}F_m) = 0 \quad (6)$$

$$\Delta H_k(\mathbf{E},\mathbf{F}) = \frac{\left(P^{sp}_k F_k - Q^{sp}_k E_k\right)}{\left(E_k^2+F_k^2\right)} - \sum_{m\in\kappa}(G_{km}F_m + B_{km}E_m) = 0$$

$$\Delta P_k(\mathbf{E},\mathbf{F}) = P^{sp}_k - \sum_{m\in\kappa}[E_k(G_{km}E_m - B_{km}F_m) + F_k(G_{km}F_m + B_{km}E_m)] = 0 \quad (7)$$

$$\left(V^{sp}_k\right)^2 = E_k^2 + F_k^2 \quad (8)$$

In the active power balance equation, the bus voltages are written in polar coordinates. Injected powers and nodal admittance matrix elements are represented in rectangular coordinates. References [18,19] proposed the use of current injection mismatches considering $\Delta Q$ as a dependent variable, together with the voltage magnitude constraint Equation (8),

both written in rectangular coordinates. In [8] a modified current injection power flow (MCIPF) considering $Q_{gen,k}$ as a function of the state variables $\theta$ and $|\mathbf{V}|$ was proposed.

The Newton-Raphson linearized equation of the PCIPF can be written as:

$$\begin{bmatrix} \Delta \mathbf{G_{pq}} \\ \Delta \mathbf{P_{pv}} \big/ \left|\mathbf{V_{pv}}\right| \\ \hline \Delta \mathbf{HI_{pq}} \end{bmatrix} = -\mathbf{J_I} \begin{bmatrix} \Delta \boldsymbol{\theta}_{\mathbf{pq}} \\ \Delta \boldsymbol{\theta}_{\mathbf{pv}} \\ \hline \Delta |\mathbf{V}|_{\mathbf{pq}} \end{bmatrix} = \left[\begin{array}{c|c} \mathbf{J_1} & \mathbf{J_2} \\ \hline \mathbf{J_3} & \mathbf{J_4} \end{array}\right] \begin{bmatrix} \Delta \boldsymbol{\theta}_{\mathbf{pq}} \\ \Delta \boldsymbol{\theta}_{\mathbf{pv}} \\ \hline \Delta |\mathbf{V}|_{\mathbf{pq}} \end{bmatrix} \tag{9}$$

where the Jacobian matrix ($\mathbf{J_I}$) has the same structure of $\mathbf{J}$, for $npq$ load buses and $npv$ generator buses. Submatrices $\mathbf{J_1} = -\partial \Delta \mathbf{G_{pq}}(\theta, |\mathbf{V}|)/\partial\theta$, $\mathbf{J_2} = -\partial \Delta \mathbf{G_{pq}}(\theta, |\mathbf{V}|)/\partial |\mathbf{V}|$, $\mathbf{J_3} = -\partial \Delta \mathbf{HI_{pq}}(\theta, |\mathbf{V}|)/\partial\theta$ and $\mathbf{J_4} = -\partial \Delta \mathbf{HI_{pq}}(\theta, |\mathbf{V}|)/\partial |\mathbf{V}|$ for PQ buses and $\mathbf{J_1} = -\partial(\Delta \mathbf{P_{pv}}(\theta, |\mathbf{V}|)/|\mathbf{V_{pv}}|)/\partial\theta$, $\mathbf{J_2} = -\partial(\Delta \mathbf{P_{pv}}(\theta, |\mathbf{V}|)/|\mathbf{V_{pv}}|)/\partial |\mathbf{V}|$ for PV buses are given by:

Submatrix $\mathbf{J_1}$ for PQ buses:

$$J_1(k,i) = -|V_i||Y_{ki}| \sin(\varphi_{ki} + \theta_i) \text{ for } k \neq i \tag{10}$$

$$J_1(k,k) = -|V_k||Y_{kk}| \sin(\varphi_{kk} + \theta_k) + \frac{\left|S_k^{sp}\right|}{|V_k|} \sin(-\varphi_k + \theta_k) \tag{11}$$

and for PV buses:

$$J_1(k,i) = -|V_i||Y_{ki}| \sin(\varphi_{ki} - \theta_{ki}) \text{ for } k \neq i \tag{12}$$

$$J_1(k,k) = -|V_k||Y_{kk}| \sin(\varphi_{kk}) - \frac{Q_k}{|V_k|} \tag{13}$$

Submatrix $\mathbf{J_2}$ for PQ buses:

$$J_2(k,i) = |Y_{ki}| \cos(\phi_{ki} + \theta_i) \text{ for } k \neq i \tag{14}$$

$$J_2(k,k) = |Y_{kk}| \cos(\phi_{kk} + \theta_k) + \frac{\left|S_k^{sp}\right|}{|V_k^2|} \cos(-\varphi_k + \theta_k) \tag{15}$$

and for PV buses:

$$J_2(k,i) = |Y_{ki}| \cos(\phi_{ki} - \theta_{ki}) \text{ for } k \neq i \tag{16}$$

Submatrix $\mathbf{J_3}$ for PQ buses:

$$J_3(k,i) = |V_i||Y_{ki}| \cos(\phi_{ki} + \theta_i) \text{ for } k \neq i \tag{17}$$

$$J_3(k,k) = |V_k||Y_{kk}| \cos(\phi_{kk} + \theta_k) - \frac{\left|S_k^{sp}\right|}{|V_k|} \cos(-\varphi_k + \theta_k) \tag{18}$$

Submatrix $\mathbf{J_4}$ for PQ buses:

$$J_4(k,i) = |Y_{ki}| \sin(\phi_{ki} + \theta_i) \text{ for } k \neq i \tag{19}$$

$$J_4(k,k) = |Y_{kk}| \sin(\phi_{kk} + \theta_k) + \frac{\left|S_k^{sp}\right|}{|V_k^2|} \sin(-\varphi_k + \theta_k) \tag{20}$$

For arbitrarily chosen initial values of $\theta$ and $|\mathbf{V}|$, the mismatches are computed by Equation (1) for PQ buses, and by Equation (5) for PV buses. If their maximum absolute values are smaller than an adopted tolerance, the solution was obtained. Otherwise, solve

Equation (9) to obtain the correction vectors ($\mathbf{\Delta\theta}$ and $\Delta|\mathbf{V}|$) and update their values as follows:

$$\begin{aligned} \theta^{v+1} &= \theta^{v} + \mathbf{\Delta\theta}^{v} \\ |\mathbf{V_{pq}}|^{v+1} &= |\mathbf{V_{pq}}|^{v} + \mathbf{\Delta}|\mathbf{V_{pq}}|^{v} \end{aligned} \tag{21}$$

where v is an iteration counter.

In this formulation, as in the standard method, while the generated reactive powers of PV buses lie within the maximum and minimum limits, their respective equations ($\Delta HI_k(\theta, |\mathbf{V}|)$ and elements of $\mathbf{J_3}$ and $\mathbf{J_4}$ are not included in Equation (9), as well as the elements of $\mathbf{J_2}$ and $\mathbf{J_4}$ corresponding to the derivatives with respect to voltage magnitudes of PV buses since their voltage magnitudes are specified. Therefore, the total number of equations and then the structure and size of the Jacobian matrix remain the same as in the standard method.

## 3. BX Version of Current Injection Fast Decoupled Power Flow

Simplifications introduced in the Jacobian matrix by Stott and Alsac [23] led to the XB version of the Fast Decoupled Power Flow (FDPF) method. In [25], the BX version, hereafter referred to as the standard fast decoupled power flow (SFDPF-BX), has been implemented and tested. The basic difference among the versions is in the elements of matrices $\mathbf{B'}$ and $\mathbf{B''}$ [26]. The BX version of PCIPF, hereafter named as proposed current injection fast decoupled power flow (PCIFDPF-BX), is obtained by considering a flat-start ($|V_k| = |V_i| = 1.0$ p.u. and $\theta_k = \theta_i = 0$) and ${P_k}^{sp}$ and ${Q_k}^{sp}$ equal to their respective active, Equation (22), and reactive, Equation (23), powers.

$$P_k(\theta, |\mathbf{V}|) = G_{kk}|V_k|^2 + |V_k| \sum_{i \in \Omega_k} |Y_{ki}||V_i| \cos(\phi_{ki} - \theta_{ki}) \tag{22}$$

$$Q_k(\theta, |\mathbf{V}|) = -B_{kk}|V_k|^2 - |V_k| \sum_{i \in \Omega_k} |Y_{ki}||V_i| \sin(\phi_{ki} - \theta_{ki}) \tag{23}$$

Applying those considerations to Equations (10) through (20), the diagonal and off-diagonal elements of submatrices $\mathbf{J_1}$, $\mathbf{J_2}$, $\mathbf{J_3}$, and $\mathbf{J_4}$ are:
Submatrix $\mathbf{J_1}$ for PQ and PV buses:

$$J_1(k,i) = -B_{ki} \quad \text{for } k \neq i \tag{24}$$

$$J_1(k,k) = -B_{kk} - Q_k^{sp} = -B_{kk} - (-B_{kk} - \sum_{i \in \Omega_k} B_{ki}) = \sum_{i \in \Omega_k} B_{ki} \tag{25}$$

Submatrix $\mathbf{J_2}$ for PQ buses:

$$J_2(k,i) = G_{ki} \quad \text{for } k \neq i \tag{26}$$

$$J_2(k,k) = G_{kk} + P_k^{sp} = G_{kk} + (G_{kk} + \sum_{i \in \Omega_k} G_{ki}) = G_{kk} \tag{27}$$

and for PV buses:

$$J_2(k,i) = G_{ki} \quad \text{for } k \neq i \tag{28}$$

Submatrix $\mathbf{J_3}$ for PQ buses:

$$J_3(k,i) = G_{ki} \quad \text{for } k \neq i \tag{29}$$

$$J_3(k,k) = G_{kk} - P_k^{sp} = G_{kk} - (G_{kk} + \sum_{i \in \Omega_k} G_{ki}) = -\sum_{i \in \Omega_k} G_{ki} = G_{kk} \tag{30}$$

Submatrix $\mathbf{J_4}$ for PQ buses:

$$J_4(k,i) = B_{ki} \quad \text{for } k \neq i \tag{31}$$

$$J_4(k,k) = B_{kk} - Q_k^{sp} = 2B_{kk} + \sum_{i \in \Omega_k} B_{ki} = -\sum_{i \in \Omega_k} B_{ki} + 2(b_k^{sh} + \sum_{i \in \Omega_k} b_{ki}^{sh}) \tag{32}$$

where $G_{ki}$, $G_{kk}$, $B_{ki}$, and $B_{kk}$ are the real and imaginary parts of the bus admittance matrix $\mathbf{Y}$, $\Omega_k$ is the set of buses directly connected to bus k, $b_k^{sh}$ is the susceptance of shunt element at bus k, and $b_{ki}^{sh}$ is the line charging between buses k and i. The proposed BX version of the fast decoupled load flow method is given by:

$$\begin{bmatrix} \Delta \mathbf{G_{pq}} \\ \Delta \mathbf{P_{pv}} / |\mathbf{V_{pv}}| \end{bmatrix} = \mathbf{B}' \begin{bmatrix} \Delta \theta_{\mathbf{pq}} \\ \Delta \theta_{\mathbf{pv}} \end{bmatrix} \tag{33}$$

$$[\Delta \mathbf{HI_{pq}}] = \mathbf{B}'' [\Delta |\mathbf{V_{pq}}|] \tag{34}$$

where the off-diagonal and diagonal elements of matrix $\mathbf{B}'$ are given by Equation (24) and Equation (25), respectively. Note from Equation (24) and Equation (25) that shunt elements do not appear in the derivations. For radial systems and meshed systems with constant R/X ratio, the elements of matrix $\mathbf{B}'' = \mathbf{J_4} - \mathbf{J_3}(\mathbf{J_1})^{-1}\mathbf{J_2}$, computed for flat start as in Equations (24) through (32), are given by:

$$B''(k,i) = x_{ki}^{-1} \quad \text{for } k \neq i \tag{35}$$

$$B''(k,k) = -\sum_{i \in \Omega_k} x_{ki}^{-1} + 2(b_k^{sh} + \sum_{i \in \Omega_k} b_{ki}^{sh}) \tag{36}$$

Note that double shunts naturally appear during the derivations, so we do not have to "double" them afterwards [26].

## 4. Test Results

Numerical tests were conducted for the 57-, 118- and 300-bus IEEE test systems, as well as for a realistic 787-bus system, to compare the proposed current injection Newton-Raphson (PCIPF) and its corresponding BX version of current injection fast decoupled power flow (PCIFDPF-BX) with their respective power injection versions (SPF and SFDPF-BX). For all methods, the maximum absolute value of the power mismatch vector $\mathbf{R} = [\Delta \mathbf{P}^T \ \Delta \mathbf{Q}^T]^T$ ($||\mathbf{R}||_\infty = \max\{|R_i|\}$) is adopted as the convergence criterion. The convergence threshold adopted for the maximum mismatch was $10^{-4}$ p.u. Reactive power generation limits at PV buses were enforced in all methods.

The computational time associated with a computer code depends on several aspects. Among them, one could mention the processor, the allocated memory, the computer language, and the programmer's style, to name a few. All simulations presented in this paper were carried out using Matlab®, which is an interpreted language (as opposed to C, which is a compiled language), thus yielding larger times. Of course, a production-grade implementation of the proposed method would have to be done in a compiled language. Regarding the different implementations presented in Tables 1–8, we have assured that:

They are as fair as possible, that is, we attempted to keep the same core of the code, and made the strictly necessary changes to implement each one.

All simulations were run on the same computer, and the same version of Matlab®.

Therefore, we believe that it is fair to say that, under these conditions, the number of iterations represents quite faithfully the efficiency of each method. Thus, Newton's method version that converges in four iterations is faster than another one that converges in five or six iterations.

As far as the comparison of computer times between Newton's and Fast Decoupled methods, we rely on [23], where the authors estimated that a full iteration of the Fast decoupled power flow (P half-iteration plus Q half-iteration) takes one-fifth of Newton's method.

To illustrate the iterative process convergence, all iterative power flow processes starts from the respective power system data files and the total mismatch is used. This mismatch is defined as the sum of the absolute values of the active and reactive power mismatches. As for the decoupled versions, the standard iteration scheme was used [23]. Furthermore, all the tests with the SFDPF-BX have been conducted using normalized mismatches (ΔP/V and ΔQ/V) [26]. In order to highlight the convergence similarities between the fast decoupled

power flow methods, a larger number of half-iterations, Pθ and QV, were allowed in the simulations. As for the Newton methods, a maximum of 20 full iterations was adopted.

Different loading conditions and R/X transmission line ratios are considered to carry out the performance assessment. For the R/X ratio tests, parameters R and X of all branches varied according to multipliers shown in the first columns of the respective tables. As for the loading tests, the active and reactive loads and active power generations varied according to a loading factor (λ), shown in the first columns of the respective tables.

The strategy proposed in [27] is based on evidence that the lower the R/X ratio (the stronger the P-θ and Q-V decoupling), the better the performance of decoupled PF methods based on power injection. In [28], the influence of the R/X ratio is discussed and incorporated in the determination of the base angle ($\phi_{base}$) in electrical systems.

### *4.1. Performance of the Methods for the IEEE Test Systems*

The performance of the methods to obtain the solution considering different loading conditions and a fixed R/X ratio of $1_x$R/$1_x$X, are presented in Tables 1 and 2. The maximum loading factor values ($\lambda_{max}$) for the 57- and 118-bus systems were 1.5972 and 1.8664 p.u., respectively, as previously obtained using the continuation power flow presented in [29], and later used to properly choose the loading factor values presented in the first column of the tables. The P-V curves were traced considering the loads modeled as constant power and using the loading factor (λ) to simulate the active and reactive load increment, considering a constant power factor and an equivalent active power generation increase [3]. From the results presented in Tables 1 and 2, it is observed that all the methods, including the proposed PCIPF, presented similar performances. All of them show an increase in the number of iterations as the systems approach their respective maximum loading points (MLP), failing to converge for loadings equal to or slightly higher than their respective MLP. As far as the decoupled methods, both present practically the same performance and, likewise the Newton's methods, they also present a larger number of iterations as the system approaches the maximum loading point.

**Table 1.** IEEE 57-bus system: performance for different loading conditions.

| λ (p.u.) | SPF | MCIPF | PCIPF | SFDPF-BX Pθ/QV | PCIFDPF-BX Pθ/QV |
|---|---|---|---|---|---|
| 1.0 | 4 | 4 | 4 | 8-8 | 8-8 |
| 1.4 | 5 | 5 | 5 | 10-9 | 11-11 |
| 1.5 | 5 | 5 | 5 | 12-11 | 13-13 |
| 1.58 | 6 | 6 | 6 | 21-20 | 23-22 |
| 1.596 | 7 | 7 | 7 | 41-40 | 44-43 |
| 1.6 | NC | NC | NC | NC | NC |

NC—no convergence considering the maximum number of iterations.

**Table 2.** IEEE 118-bus system: performance for different loading conditions.

| λ (p.u.) | SPF | MCIPF | PCIPF | SFDPF-BX Pθ/QV | PCIFDPF-BX Pθ/QV |
|---|---|---|---|---|---|
| 1.0 | 4 | 4 | 4 | 8-8 | 9-8 |
| 1.4 | 5 | 5 | 5 | 9-9 | 9-9 |
| 1.7 | 6 | 6 | 6 | 12-12 | 13-13 |
| 1.86 | 8 | 8 | 8 | 51-50 | 41-40 |
| 1.865 | 8 | 8 | 8 | 82-81 | 49-48 |
| 1.9 | NC | NC | NC | NC | NC |

The numbers of iterations for the 57- and 118-bus systems, considering different R/X ratios, are presented in Tables 3 and 4. For both systems, all methods present a low number of iterations, except for the PCIFDPF-BX, that requires more iterations for $3_x$R/$1_x$X of the 57-bus system. Both methods fail to converge for R multipliers equal to or greater than four.

**Table 3.** IEEE 57-bus system: performance for different R/X ratios.

| R/X Ratios | SPF | MCIPF | PCIPF | SFDPF-BX Pθ/QV | PCIFDPF-BX Pθ/QV | $\lambda_{max}$ (p.u.) |
|---|---|---|---|---|---|---|
| $1.0_xR/0.5_xX$ | 3 | 3 | 4 | 11-10 | 13-12 | 2.2296 |
| $1.0_xR/1.0_xX$ | 4 | 4 | 4 | 8-8 | 8-8 | 1.5972 |
| $2.0_xR/1.0_xX$ | 5 | 5 | 5 | 10-10 | 17-16 | 1.3444 |
| $3.0_xR/1.0_xX$ | 8 | 8 | 7 | 13-21 | 44-44 | 1.1104 |
| $4.0_xR/1.0_xX$ | NC | NC | NC | NC | NC | 0.9339 |

**Table 4.** IEEE 118-bus system: performance for different R/X ratios.

| R/X Ratios | SPF | MCIPF | PCIPF | SFDPF-BX Pθ/QV | PCIFDPF-BX Pθ/QV | $\lambda_{max}$ (p.u.) |
|---|---|---|---|---|---|---|
| $1.0_xR/0.5_xX$ | 5 | 5 | 5 | 11-10 | 10-10 | 2.5868 |
| $1.0_xR/1.0_xX$ | 4 | 4 | 4 | 8-8 | 9-8 | 1.8664 |
| $2.0_xR/1.0_xX$ | 5 | 5 | 5 | 10-9 | 10-10 | 1.6228 |
| $3.0_xR/1.0_xX$ | 5 | 5 | 6 | 10-10 | 13-13 | 1.2371 |
| $4.0_xR/1.0_xX$ | NC | NC | NC | NC | NC | 0.9154 |

Figure 1a,b show the converged states (θ, |V|) obtained by the methods for the $3_xR/1_xX$ condition of the 118-bus system. At the end of the iterative process, all methods converged to the same solution. The respective total power mismatches convergence characteristic can be seen in Figure 1c. Comparing evolution of the mismatches for the proposed methods with that of their respective standard methods, it can be seen that the proposed methods present good convergence characteristics.

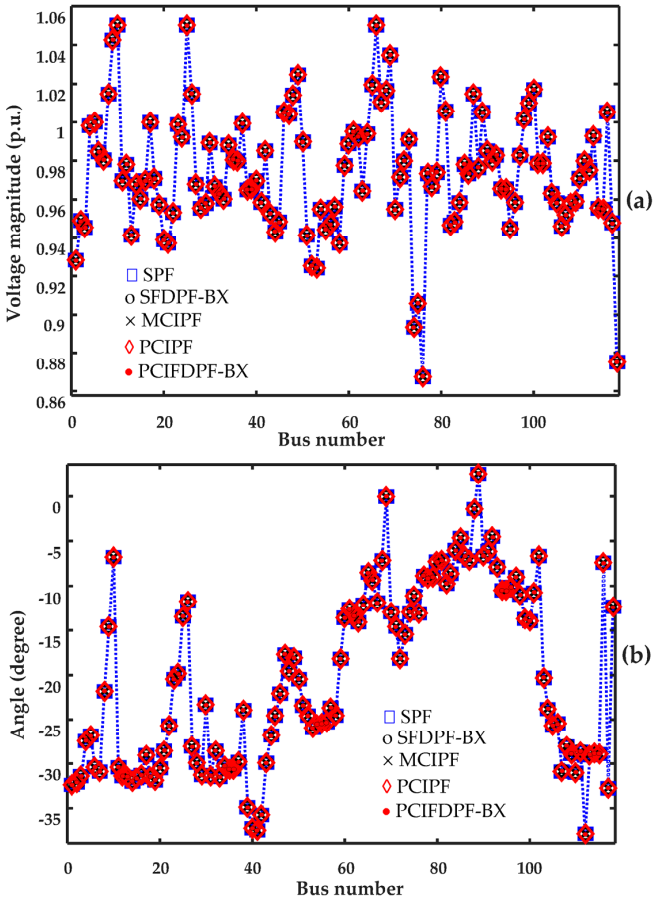


**Figure 1.** *Cont.*

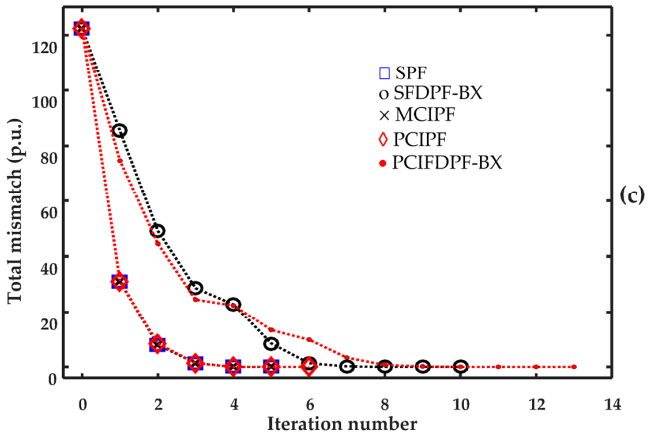


**Figure 1.** IEEE 118-bus system: (**a**) voltage magnitude, and (**b**) angle profiles, and (**c**) evolution of total mismatches of each one of the methods, for the $3_xR/1_xX$ ratio.

Table 5 shows the performances for different loading conditions of the 300-bus system. This system presents a heavy loading condition at base case, with an MLP equal to 1.0553 p.u., which is very close to the base case operating point (λ = 1.0 p.u.). All methods succeed in finding a solution, even for values close to the maximum loading point ($\lambda_{max}$ = 1.0553 p.u.), failing only for values equal to or slightly higher than it.

The converged operating states obtained by all methods for each loading condition presented in Table 6 are the same. The voltage magnitude of the critical bus obtained by each method is plotted on the same P-V curve, as shown in Figure 2a.

The trajectories of IEEE 300-bus total power mismatches for λ = 1.05 p.u. and R/X condition of $1.0_xR/1_xX$ are shown in Figure 2b. As in the case of IEEE 118-bus system, the proposed methods present practically the same convergence behavior of their respective standard methods. For all of them, the total power mismatches are strongly reduced during the first five iterations. Nevertheless, the decoupled methods require more iterations than Newton's methods to obtain the solution, most of them spent calculating it with the accuracy desired.

The performances of the methods for the IEEE 300-bus system, considering different R/X factors, are shown in Table 6. From the results, both Newton's methods (MCIPF and PCIPF) showed similar performance, when compared with the standard version (SPF), the PCIPF being a bit more efficient. As far as the decoupled versions, the proposed PCIFDPF-BX presents better performance than the standard (SFDPF-BX), except for the $1.0_xR/0.5_xX$ condition. As illustrated in [8] and in the last column of Table 6, the R multiplier 1.473 corresponds to a maximum loading value, therefore, this is the reason why the methods do not converge for an R multiplier equal to or slightly higher than it (1.473). It is well-known that the convergence problems encountered by the methods presented in [8], and also in this paper, to obtain the maximum loading point (MLP) arise from numerical difficulties associated with the Jacobian matrix (**J**) conditioning. For systems with constant PQ loads, the gradual load increment will lead to a saddle-node bifurcation, which also corresponds to the maximum loading point (MLP). Under these conditions, the PF Jacobian matrix will become singular and, consequently, the use of conventional methods, like Newton's method and its variants (such as the fast-decoupled method) will show numeric difficulties.

**Table 5.** IEEE 300-bus system: performance for different loading conditions.

| λ (p.u.) | SPF | MCIPF | PCIPF | SFDPF-BX Pθ/QV | PCIFDPF-BX Pθ/QV |
|---|---|---|---|---|---|
| 1.0 | 4 | 4 | 4 | 13-12 | 13-12 |
| 1.02 | 4 | 4 | 4 | 16-15 | 15-14 |
| 1.04 | 5 | 5 | 5 | 24-23 | 22-21 |
| 1.05 | 5 | 5 | 5 | 36-35 | 32-32 |
| 1.055 | 7 | 7 | 7 | 80-80 | 74-73 |
| 1.056 | NC | NC | NC | NC | NC |

**Table 6.** IEEE 300-bus system: performance for different R/X ratios.

| R/X Ratios | SPF | MCIPF | PCIPF | SFDPF-BX Pθ/QV | PCIFDPF-BX Pθ/QV | $\lambda_{max}$ (p.u.) |
|---|---|---|---|---|---|---|
| $1.0_xR/0.5_xX$ | 5 | 6 | 4 | 7-7 | 16-18 | 1.4303 |
| $1.0_xR/1.0_xX$ | 4 | 4 | 4 | 13-12 | 12-12 | 1.0553 |
| $1.2_xR/1.0_xX$ | 5 | 5 | 4 | 17-16 | 15-15 | 1.0292 |
| $1.4_xR/1.0_xX$ | 6 | 5 | 5 | 28-27 | 25-25 | 1.0086 |
| $1.47_xR/1.0_xX$ | 7 | 7 | 6 | 79-77 | 70-69 | 1.0002 |
| $1.473_xR/1.0_xX$ | NC | NC | NC | NC | NC | 0.9998 |

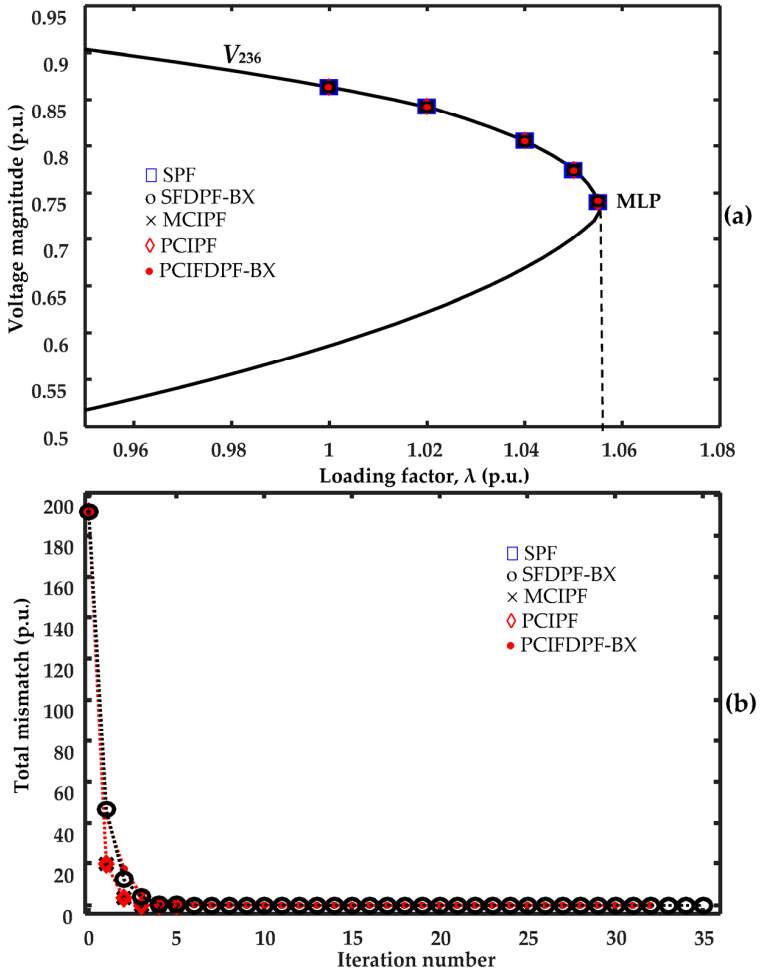


**Figure 2.** IEEE 300-bus system: (**a**) P-V curve of critical bus, and (**b**) evolution of total mismatches, for λ = 1.05 p.u. and $1.0_xR/1.0_xX$.

*4.2. Performance of the Methods for the Real, Large Systems*

The objective of this section is to show the performance of the proposed current injection Newton (PCIPF) and fast decoupled power flow methods (PCIFDPF-BX) for a real, large system of 787 buses, and 1395 branches.

The effects of the increment on the loading factor are shown in Table 7. For this system, the maximum loading factor is equal to 1.1272. The maximum loading point and P-V curve were previously obtained using the continuation power flow presented in [29]. Figure 3a shows the converged voltage magnitudes of the critical bus (576) plotted on the P-V curves, for each loading condition presented in the first column of Table 7.

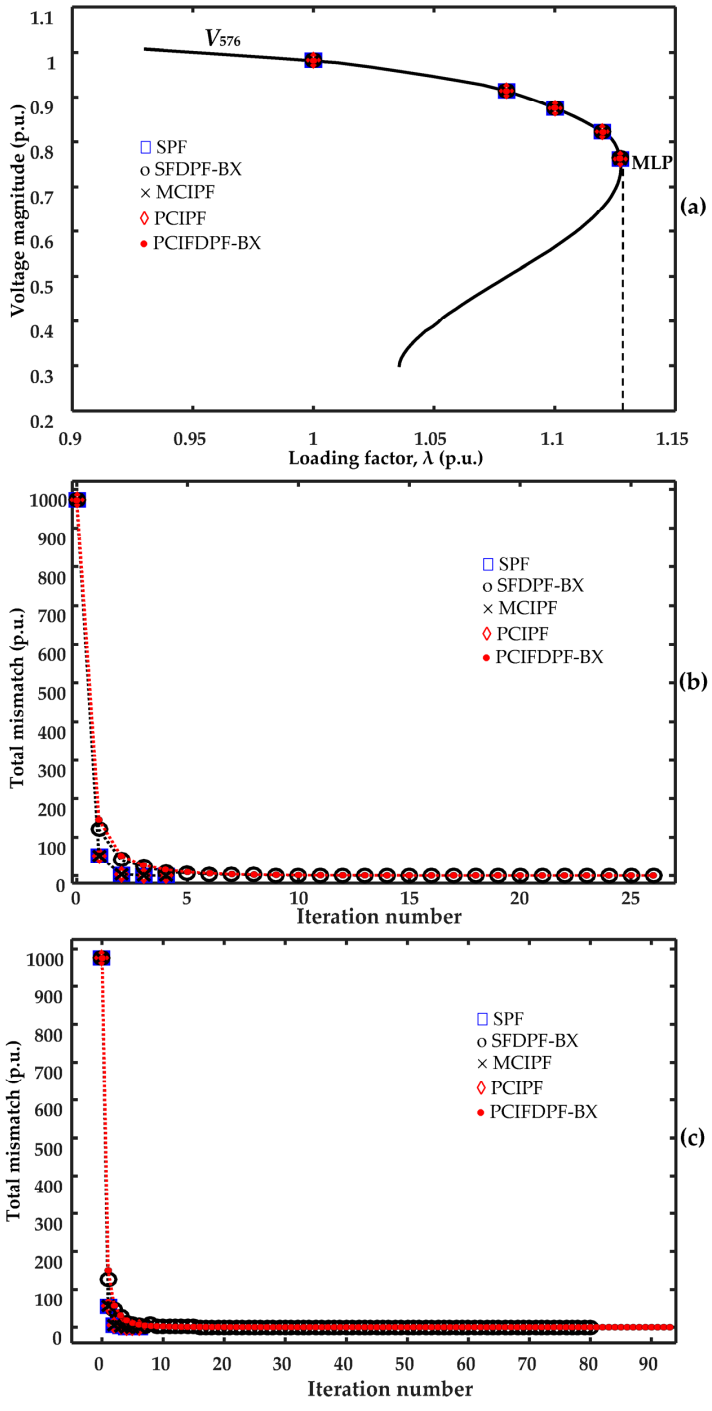


**Figure 3.** System of 787 buses: (**a**) P-V curve of critical bus, and evolution of total mismatches, for (**b**) λ = 1.12 p.u. and $1.0_xR/1.0_xX$, and for (**c**) λ = 1.127 p.u. and $1.0_xR/1.0_xX$.

The results confirm that the converged state obtained by each method is the same. Figure 3b depicts the total power mismatch trajectories for λ = 1.12 p.u. and $1.0_xR/1.0_xX$ conditions. The Newton methods, including the PCIPF, need four iterations to obtain the solution, whereas the decoupled methods require 26 Pθ and QV half-iterations for convergence. The total mismatch evolution is presented in Figure 3b. It can be seen again that the decoupled methods quickly approach the solution, spending less than five iterations, and afterwards spend most of the total iterations to calculate it with the accuracy desired. As shown in Figure 3c, this also happens for the next loading factor, but at the expense of a considerable increase in the number of iterations, as a result of being closer to the maximum loading point.

**Table 7.** System of 787 buses: performance for different loading conditions.

| λ (p.u.) | SPF | MCIPF | PCIPF | SFDPF-BX Pθ/QV | PCIFDPF-BX Pθ/QV |
|---|---|---|---|---|---|
| 1.000 | 3 | 3 | 3 | 8-8 | 10-9 |
| 1.080 | 4 | 4 | 4 | 14-15 | 15-15 |
| 1.100 | 5 | 5 | 5 | 18-19 | 18-18 |
| 1.120 | 4 | 4 | 4 | 26-26 | 26-26 |
| 1.127 | 6 | 6 | 6 | 95-94 | 92-93 |
| 1.1274 | NC | NC | NC | NC | NC |

The effects of the increment on the R/X ratios are shown in Table 8, from where it can be seen that as the R/X ratio increases, the PICPF presents the same performance of the other Newton methods, while the decoupled methods converge more slowly, with the PCIFDPF being the most affected, not converging for R multiplier equal to or higher than 2.4. Note that in the last column of Table 8, as the ratio R/X increases, the system approaches the corresponding maximum loading value ($\lambda_{max}$), and this is the main reason why all the methods do not converge. This is also related to the singularity of the **J** matrix at the MLP (zero eigenvalues).

**Table 8.** System of 787 buses: performance for different R/X ratios.

| R/X Ratios | SPF | MCIPF | PCIPF | SFDPF-BX Pθ/QV | PCIFDPF-BX Pθ/QV | MCIFDPF-BX Pθ/QV (α) | $\lambda_{max}$ (p.u.) |
|---|---|---|---|---|---|---|---|
| $1.0_xR/0.5_xX$ | 4 | 4 | 4 | 15-17 | 16-17 | 15-16 (4.535°) | 1.7863 |
| $1.0_xR/1.0_xX$ | 3 | 3 | 3 | 8-8 | 10-9 | 10-9 (1.003°) | 1.1272 |
| $2.0_xR/1.0_xX$ | 4 | 4 | 4 | 14-17 | 38-34 | 16-15 (31.604°) | 1.0596 |
| $2.2_xR/1.0_xX$ | 4 | 4 | 4 | 19-18 | NC | 21-20 (40.280°) | 1.0361 |
| $2.4_xR/1.0_xX$ | 5 | 5 | 5 | 35-34 | NC | 36-36 (50.925°) | 1.0113 |
| $2.45_xR/1.0_xX$ | 6 | 6 | 6 | 51-51 | NC | 52-52 (54.030°) | 1.0047 |
| $2.48_xR/1.0_xX$ | 7 | 7 | 7 | 80-80 | NC | 111-111 (56.02°) | 1.0008 |
| $2.486_xR/1.0_xX$ | NC | NC | NC | NC | NC | NC | 0.99996 |

One of the reasons for the non-convergence of the proposed method (PCIFDPF-BX) is related to the use of the voltage angle ($\theta_k$) in the equations of the current injection method, Equations (3) and (4), instead of the voltage angle differences ($\theta_{ki}$), as is the case with the equations of the power injection method. Figure 4a,b present the respective bus voltage angles and the angle difference across the lines, for the base case, λ = 1.0 p.u. and $1.0_xR/1.0_xX$, while Figure 5a,b presents the bus voltage angles and the angle difference across the lines for λ = 1.0 p.u. and $2.4_xR/1.0_xX$.

From Figures 4a and 5a and the last column of Table 8, as the R/X ratio increases, the bus voltage phase angles also increase, while the maximum loading point decreases. As a consequence, the system is brought to a state in which the conditions for reliable convergence of fast decoupled power flows may not be satisfied, resulting in a slow convergence. In [30], a criterion was proposed to select a new slack bus to result in a

smaller angle difference across the lines and, therefore, a better convergence of standard fast decoupled power flow. The strategy proposed in this paper is based on the analysis that follows.

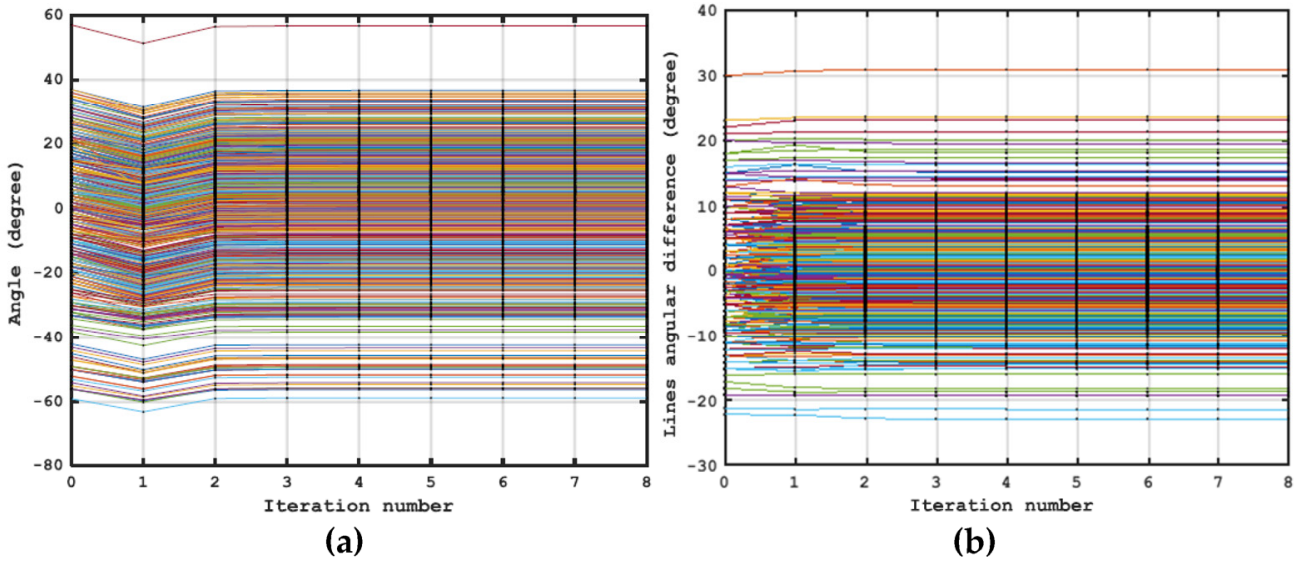


**Figure 4.** System of 787 buses: (**a**) bus voltage angles, and (**b**) lines angular difference for the base case condition: $\lambda$ = 1.0 p.u. and $1.0_{x}$R/$1.0_{x}$X.

From Figures 4a and 5a, it can be observed that the PCIFDPF-BX presents a better performance when the angles remain in a more restricted range ($\pm 60^{o}$), and there is a symmetry with respect to the horizontal axis. Besides, the analyses of the evolution of the total mismatches had shown that, in general, the proposed decoupled method spent less than five iterations to approach the adopted convergence criterion. Therefore, to improve the performance of the PCIFDPF-BX, the strategy proposed in this paper is to add an angle $\alpha$ to all bus voltage angles ($\theta$) at a certain iteration (eighth in this case), aiming to obtain a symmetry with respect to the horizontal axis and also restrict the voltage angle range, see Figure 5c. For these purposes, the value of angle $\alpha$ will be given by Equation (37):

$$\alpha = \frac{|\theta_{\min} - \theta_{\max}|}{2} - \theta_{\max} \tag{37}$$

where $\theta_{\min}$ and $\theta_{\max}$ are, respectively, the minimum and maximum bus voltage angles in that iteration. After convergence the actual voltage angles are computed by:

$$\theta_i^{\text{actual}} = \theta_i^{\text{converged}} - \alpha, \text{ for } i = 1, \cdots, \text{NB} \tag{38}$$

where NB is the total number of system buses. This proposed approach will be hereafter named as modified current injection fast decoupled power flow (MCIFDPF-BX).

Column seven of Table 8 presents the results of the proposed modification using the MCIFDPF-BX. As can be seen from the results, the proposed strategy improves the convergence of PCIFDPF-BX for R/X ratio higher than $2.0_{x}$R/$1.0_{x}$X.

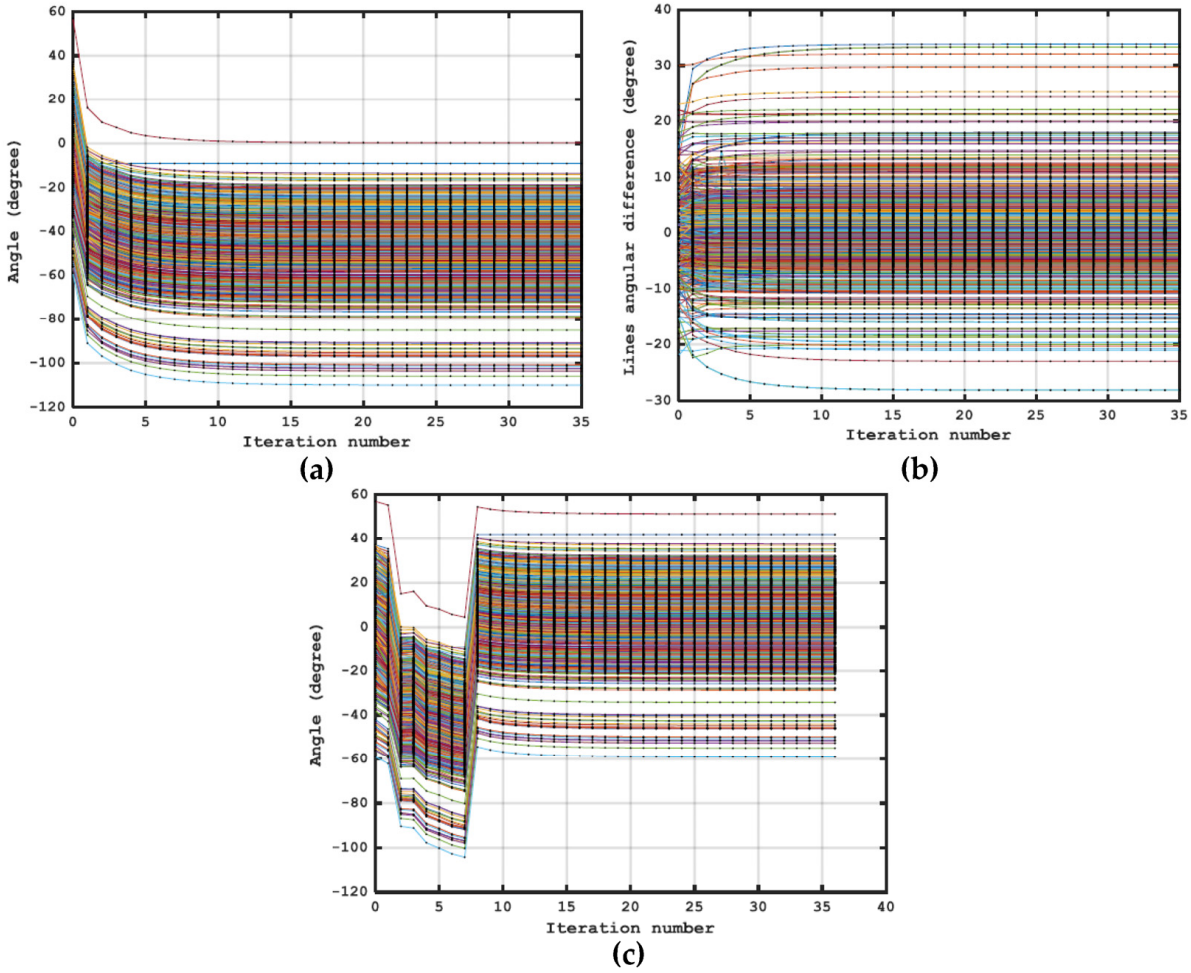


**Figure 5.** System of 787 buses: (**a**) bus voltage angles for λ = 1.0 p.u. and $2.4_xR/1.0_xX$ condition, (**b**) lines angular difference for λ = 1.0 p.u. and $2.4_xR/1.0_xX$ condition, and (**c**) with the addition in the eighth iteration of 50.93° at all bus voltage angles.

## 5. Conclusions

In this work the development of a Newton-Raphson and a BX version of fast decoupled power flow methods based on current injection equations written in polar coordinates is presented. Their performances are compared with their respective Newton and fast decoupled power injection standard versions, which are also written in polar coordinates. Performance comparisons were made for various loading conditions and different R/X ratios on the 57-, 118- and 300-bus IEEE test systems, as well as on a realistic 787-bus system. The simulation results showed that the performance of the proposed Newton-Raphson current injection method is similar (an average of five iterations to obtain each point on the P-V curve) to its respective power injection version. The increase in the R/X ratio approaches the system to the corresponding maximum loading value, and this is the main reason why all methods do not converge, and for larger ratios being the decoupled methods most affected. For the 787-bus system, the proposed BX version of the fast decoupled power flow method does not converge for an R multiplier equal to or higher than 2.4. Besides the effect of reducing the maximum loading point consequent of R/X ratio increase, it was verified that the current injection fast decoupled power flow BX version is more affected due to the use of the bus k voltage angle, instead of the voltage angle difference, as in the case of power injection fast decoupled power flow BX version. A proposed strategy, consisting of adding, in a certain iteration, an angle to all buses provided a convergence improvement, as a consequence of obtaining symmetry with respect to the horizontal axis, and also a reduction in the voltage angle range.

**Author Contributions:** C.C.d.O.: Conceptualization, Writing—Original Draft, Writing—Review and Editing, Investigation. A.B.N.: Conceptualization, Writing—Original Draft, Writing—Review and Editing, Investigation. D.A.A.: Conceptualization, Writing—Original Draft, Writing—Review and Editing, Investigation. C.R.M.: Writing—Review and Editing, Funding Acquisition, Supervision. C.A.C.: Conceptualization, Writing—Original Draft, Writing—Review and Editing, Investigation. All authors have read and agreed to the published version of the manuscript.

**Funding:** This research received no external funding.

**Data Availability Statement:** No data is used in this article.

**Acknowledgments:** The authors are grateful for the financial support provided by Brazilian Research Funding Agencies CNPq processes 408630/2018-3 and 302896/2022-8, FAPESP process 2018/12353-9, and CAPES (Coordination for the Improvement of Higher Education Personnel)—Financing Code 001.

**Conflicts of Interest:** The authors declare that they have no competing interest.

## Nomenclature

| | |
|---|---|
| PF | Power flow |
| SPF | Standard power flow |
| PCIPF | Proposed current injection power flow |
| MCIPF | Modified current injection power flow |
| FDPF | Fast decoupled power flow |
| SFDPF-BX | Standard fast decoupled power flow—BX version |
| PCIFDPF-BX | Proposed current injection fast decoupled power flow—BX version |
| MCIFDPF-BX | Modified current injection fast decoupled power flow—BX version |
| MLP | Maximum loading point |
| P-V | Voltage versus active power curve |
| PV | Generation bus |
| PQ | Load bus |
| $\lambda$ | Loading factor |
| NC | no convergence considering the maximum number of iterations. |

## Appendix A

Adding Equation (3) multiplied by $\cos(\theta_k)$ to Equation (4) multiplied by $\sin(\theta_k)$ gives:

$$\begin{aligned}&\frac{P_k^{sp}}{|V_k|} - |Y_{kk}||V_k|(\cos(\theta_k)\cos(\phi_{kk}+\theta_k) + \sin(\theta_k)\sin(\phi_{kk}+\theta_k)) - \cos(\theta_k)\sum_{i\in\Omega_k}|Y_{ki}||V_i|\cos(\phi_{ki}+\theta_i)\\ &-\sin(\theta_k)\sum_{i\in\Omega_k}|Y_{ki}||V_i|\sin(\phi_{ki}+\theta_i) = 0\end{aligned} \tag{A1}$$

The second term of the left-hand side of Equation (A1) contains the multiplication of sines and cosines. Considering the trigonometric identity $\cos(a-b) = \cos a.\cos b + \sin a.\sin b$:

$$\cos(\theta_k)\cos(\phi_{kk}+\theta_k) + \sin(\theta_k)\sin(\phi_{kk}+\theta_k) = \cos[\theta_k - (\phi_{kk}+\theta_k)] = \cos(-\phi_{kk}) = \cos(\phi_{kk})$$

which can be replaced in Equation (A1). After moving the terms $\cos(\theta_k)$ and $\sin(\theta_k)$ inside the respective summations, one gets:

$$\frac{P_k^{sp}}{|V_k|} - |Y_{kk}|\cos(\phi_{kk})|V_k| - \sum_{i\in\Omega_k}|Y_{ki}\parallel V_i|(\cos(\theta_k)\cos(\phi_{ki}+\theta_i) + \sin(\theta_k)\sin(\phi_{ki}+\theta_i)) = 0 \tag{A2}$$

Again, applying the trigonometric identity to Equation (A2):

$$\cos(\theta_k)\cos(\phi_{ki}+\theta_i) + \sin(\theta_k)\sin(\phi_{ki}+\theta_i) = \cos[\theta_k - (\phi_{ki}+\theta_i)]$$

where $\theta_k - \theta_i = \theta_{ki}$ and $\cos(\theta_{ki} - \phi_{ki}) = \cos(\phi_{ki} - \theta_{ki})$, one gets:

$$\frac{P_k^{sp}}{|V_k|} - |Y_{kk}|\cos(\phi_{kk})|V_k| - \sum_{i \in \Omega_k} |Y_{ki}||V_i|(\cos(\phi_{ki} - \theta_{ki})) = 0 \quad \text{(A3)}$$

The second term of the left-hand side of Equation (A3) is similar to the third term (summation) for $i = k$. Therefore, by incorporating the second term to the summation, one finally gets:

$$\frac{\Delta P_k}{|V_k|} = \frac{P_k^{sp}}{|V_k|} - \sum_{i \in \kappa} |Y_{ki}||V_i|(\cos(\phi_{ki} - \theta_{ki})) = 0 \quad \text{(A4)}$$

## References


1. Bonini Neto, A.; Alves, D.A.; Minussi, C.R. Artificial Neural Networks: Multilayer Perceptron and Radial Basis to Obtain Post-Contingency Loading Margin in Electrical Power Systems. *Energies* **2022**, *15*, 7939. [CrossRef]
2. Huang, Y.; Ju, Y.; Zhu, Z. An Asymptotic Numerical Continuation Power Flow to Cope with Non-Smooth Issue. *Energies* **2019**, *12*, 3493. [CrossRef]
3. Ajjarapu, V. Computational techniques for voltage stability assessment and control. In *Power Electronics and Power Systems Series*; Springer: New York, NY, USA, 2010.
4. Kulworawanichpong, T. Simplified Newton–Raphson power-flow solution method. *Int. J. Electr. Power Energy Syst.* **2010**, *32*, 551–558. [CrossRef]
5. Kamel, S.; Abdel-Akher, M.; Jurado, F. Improved NR current injection load flow using power mismatch representation of PV bus. *Int. J. Electr. Power Energy Syst.* **2013**, *53*, 64–68. [CrossRef]
6. Kamel, S.; Jurado, F.; Chen, Z.; Abdel-Akher, M.; Ebeed, M. Developed generalised unified power flow controller model in the Newton–Raphson power-flow analysis using combined mismatches method. *IET Gener. Transm. Distrib.* **2016**, *10*, 2177–2184. [CrossRef]
7. Gómez-Expósito, A.; Romero-Ramos, E.; Dzafic, I. Hybrid real-complex current injection-based load flow formulation. *Electr. Power Syst. Res.* **2015**, *119*, 237–246. [CrossRef]
8. Oliveira, C.C.; Bonini Neto, A.; Minussi, C.R.; Alves, D.A.; Castro, C.A. New Representation of PV Buses in the Current Injection Newton Power Flow. *Int. J. Electr. Power Energy Syst.* **2016**, *90*, 237–244. [CrossRef]
9. Karimi, M.; Shahriari, A.; Aghamohammadi, M.R.; Marzooghi, H.; Terzija, V. Application of Newton-based load flow methods for determining steady state condition of well and ill-conditioned power systems: A review. *Int. J. Electr. Power Energy Syst.* **2019**, *113*, 298–309. [CrossRef]
10. Matarucco, R.R.; Bonini Neto, A.; Alves, D.A. Assessment of branch outage contingencies using the continuation method. *Int. J. Electr. Power Energy Syst.* **2014**, *55*, 74–81. [CrossRef]
11. Yuan, H.; Li, F. Hybrid voltage stability assessment (VSA) for $N - 1$ contingency. *Electr. Power Syst. Res.* **2015**, *122*, 65–75. [CrossRef]
12. Wu, L.; Gao, J.; Wang, Y.; Harley, R.G. A survey of contingency analysis regarding steady state security of a power system. In Proceedings of the 2017 North American Power Symposium (NAPS), Morgantown, WV, USA, 17–19 September 2017; pp. 1–6.
13. Stott, B. Review of load-flow calculation methods. *Proc. IEEE* **1974**, *62*, 916–929. [CrossRef]
14. El-Hawary, M.E. *Electrical Power Systems: Design and Analysis*; Revised Printing, v. 2; John Wiley & Sons: Hoboken, NJ, USA, 1995; p. 799.
15. Monticelli, A.J. *Power Flow in Electric Networks*; Edgard Blucher: São Paulo, Brazil, 1983. (In Portuguese)
16. Powell, L. *Power System Load Flow Analysis*; The McGraw-Hill Education: New York, NY, USA, 2004.
17. Zhang, Y.; Lu, Y. A novel newton current equation method on power flow analysis in microgrid. In Proceedings of the 2009 IEEE Power & Energy Society General Meeting, Calgary, AB, Canada, 26–30 July 2009.
18. Da Costa, V.M.; Pereira, J.L.R.; Martins, N. An augmented Newton-Raphson power flow formulation based on current injections. *Int. J. Electr. Power Energy Syst.* **2001**, *23*, 305–312. [CrossRef]
19. Da Costa, V.M.; Martins, N.; Pereira, J.L.R. Developments in the Newton-Raphson power flow formulation based on current injections. *IEEE Trans. Power Syst.* **1999**, *14*, 1320–1326. [CrossRef]
20. Garcia, P.A.N.; Pereira, J.L.R.; Carneiro, S., Jr.; Vinagre, M.P.; Gomes, F.V. Improvements in the representation of PV buses on three-phase distribution power flow. *IEEE Trans. Power Deliv.* **2004**, *19*, 894–896. [CrossRef]
21. Dommel, H.W.; Tinney, W.F.; Powell, W.L. Further developments in Newton's method for power system applications. In *Winter Power Meeting*; Conference Paper No. 70 CP 161-PWR; IEEE: New York, NY, USA, 1970.
22. Portelinha, R.K.; Durce, C.C.; Tortelli, O.L.; Lourenço, E.M. Fast-decoupled power flow method for integrated analysis of transmission and distribution systems. *Electr. Power Syst. Res.* **2021**, *196*, 107215. [CrossRef]
23. Stott, B.; Alsac, O. Fast decoupled load Flow. *IEEE Trans. Power Appar. Syst.* **1974**, *PAS-93*, 859–869. [CrossRef]
24. Abhyankar, S.; Cui, Q.; Flueck, A.J. Fast power flow analysis using a hybrid current-power balance formulation in rectangular coordinates. In Proceedings of the 2014 IEEE PES T&D Conference and Exposition, Chicago, IL, USA, 14–17 April 2014; pp. 1–5.

25. Van Amerongen, R.A.M. A general-purpose version of the fast decoupled load flow. *IEEE Trans. Power Syst.* **1989**, *4*, 760–770. [CrossRef]
26. Monticelli, A.; Garcia, A.; Saavedra, O.R. Fast decoupled load flow: Hypothesis, derivations and testing. *IEEE Trans. Power Syst.* **1990**, *5*, 1425–1431. [CrossRef]
27. Tortelli, O.L.; Lourenço, E.M.; Garcia, A.V.; Pal, B.C. Fast decoupled power flow to emerging distribution systems via complex pu normalization. *IEEE Trans. Power Syst.* **2015**, *30*, 1351–1358. [CrossRef]
28. Portelinha, R.K.; Durcel, C.C.; Tortelli, O.L.; Lourenço, E.M.; Pal, B.C. Unified Transmission and Distribution Fast Decoupled Power Flow. *J. Control Autom. Electr. Syst.* **2019**, *30*, 1051–1058. [CrossRef]
29. Bonini Neto, A.; Alves, D.A. Improved geometric parameterisation techniques for continuation power flow. *IET Gener. Transm. Distrib.* **2010**, *4*, 1349–1359. [CrossRef]
30. Singh, S.P.; Raju, G.S.; Rao, V.S.S. A technique to improve the convergence of FDLF for systems with high R/X lines. In Proceedings of the TENCON'91. Region 10 International Conference on EC3-Energy, Computer, Communication and Control Systems, New Delhi, India, 28–30 August 1991; pp. 204–207.


**Disclaimer/Publisher's Note:** The statements, opinions and data contained in all publications are solely those of the individual author(s) and contributor(s) and not of MDPI and/or the editor(s). MDPI and/or the editor(s) disclaim responsibility for any injury to people or property resulting from any ideas, methods, instructions or products referred to in the content.